The Injection of Zonal Momentum by Buoyancy Forcing in a Southern Ocean Model

EMMA HOWARD AND ANDREW MCC. HOGG

Research School of Earth Sciences, and ARC Centre of Excellence for Climate System Science, Australian National University, Canberra, Australian Capital Territory, Australia

STEPHANIE WATERMAN

Climate Change Research Centre, and ARC Centre of Excellence for Climate System Science, University of New South Wales, Sydney, New South Wales, Australia

DAVID P. MARSHALL

Atmospheric, Oceanic and Planetary Physics, Department of Physics, University of Oxford, Oxford, United Kingdom

(Manuscript received 17 May 2014, in final form 3 October 2014)

ABSTRACT

An overturning circulation, driven by prescribed buoyancy forcing, is used to set a zonal volume transport in a reentrant channel ocean model with three isopycnal layers. The channel is designed to represent the Southern Ocean such that the forced overturning resembles the lower limb of the meridional overturning circulation (MOC). The relative contributions of wind and buoyancy forcing to the zonal circulation are examined. It is found that the zonal volume transport is strongly dependent on the buoyancy forcing and that the eddy kinetic energy is primarily set by wind stress forcing. The zonal momentum budget integrated over each layer is considered in the buoyancy-forced, wind-forced, and combined forcing case. At equilibrium, sources and sinks of momentum are balanced, but the transient spinup reveals the source of momentum for the current. In the buoyancy-forced case, the forcing creates a baroclinic shear with westward flow in the lower layer, allowing topographic form stress and bottom friction to act as the initial sources of eastward momentum, with bottom friction acting over a longer time frame. In the wind-forced and combined forcing cases, the surface wind stress dominates the initial momentum budget, and the time to reach equilibration is shorter in the combined forcing simulation. These results imply that future changes in the rate of formation of Antarctic Bottom Water may alter the volume transport of the Antarctic Circumpolar Current.

1. Introduction

The Antarctic Circumpolar Current (ACC) is the world's strongest ocean current with a zonal transport of 137 ± 7 Sverdrups (Sv; $1\ \text{Sv} \equiv 10^6\ \text{m}^3\ \text{s}^{-1}$; Meredith et al. 2011) and is the primary conduit between the major ocean basins. Strong westerly winds overlying the ACC are a potential source of eastward momentum for the mean flow, and low-resolution models of the Southern Ocean [such as general circulation models (GCMs) used for climate prediction] suggest that the strength of the ACC depends strongly on the strength of wind stress (Rintoul et al. 2001). However, this dependence becomes less pronounced as the model resolution increases, leading to the proposal of weaker relationships between ACC transport and wind stress and even the possibility that flow is "eddy saturated" and hence independent of the magnitude of wind stress (Straub 1993; Hallberg and Gnanadesikan 2006; Meredith and Hogg 2006; Munday et al. 2013).

Applying the thermal wind relation to the dynamics of Southern Ocean circulation indicates that zonal transport must be closely associated with the stratification of the ocean (Gnanadesikan and Hallberg 2000). Thus, it appears likely that the net ACC transport is simply a reflection of all processes governing the ocean stratification (Shakespeare and Hogg 2012). Surface buoyancy forcing and diapycnal mixing change the ocean density and so influence the stratification and hence the circumpolar

Corresponding author address: Andrew McC. Hogg, Research School of Earth Sciences, Australian National University, 142 Mills Rd., Acton ACT 0200, Australia.
E-mail: andy.hogg@anu.eud.au

DOI: 10.1175/JPO-D-14-0098.1

flow. Hogg (2010), Shakespeare and Hogg (2012), and Munday et al. (2013) have found that a circumpolar current in an idealized model may be driven by surface buoyancy forcing alone (provided that interior mixing is present), while Munday et al. (2011) found that changes in diapycnal mixing away from the Southern Ocean have an impact on the ACC transport and Southern Ocean overturning. If an ACC is present in models without any explicit momentum input from winds, then this raises the question of how important is momentum input from the winds in driving an ACC?

The mechanisms by which surface buoyancy forcing and interior diapycnal mixing in the ocean inject zonal momentum into the Southern Ocean remain unresolved. The lower limb in the Southern Ocean component of the meridional overturning circulation (MOC) is driven by the formation and subsequent sinking of cold, dense water masses near Antarctica. The dense water travels northward along the sloping ocean bathymetry, and previous studies have noted a strong relationship between the rate of Antarctic Bottom Water (AABW) formation and ACC transport (Gent et al. 2001; Borowski et al. 2002). The creation and sinking of AABW intensifies the stratification of the Southern Ocean and raises the isopycnal surfaces toward the southern boundary (Mazloff et al. 2013), implying a stronger ACC via the thermal wind relationship. Previous studies have not investigated how the zonal momentum is added to the system through this mechanism.

Diapycnal mixing throughout the global ocean acts to transport heat downward. In regions where heat is added to the surface of the ocean, diapycnal mixing deepens the thermocline and isopycnals (Munday et al. 2011). Taken together, the combination of surface heat flux and interior diapycnal mixing deepens isopycnals on the northern boundary of the ACC, increasing isopycnal slope in the Southern Ocean. Munday et al. (2011) hypothesize that the meridional density gradient caused by increased diapycnal mixing north of the Southern Ocean induces a northward flow at depth and a southward surface flow, which undergoes Coriolis acceleration and thereby contributes to the ACC. The induced westward momentum in the abyssal ocean opposes the ACC but is dissipated as topographic form stress, while the induced eastward momentum at the surface intensifies the ACC.

To quantitatively understand the mechanisms responsible for the response of the ACC to varying forcing conditions, it is important to understand all the sources and sinks of momentum to the circulation. Killworth and Nanneh (1994) used isopycnal coordinates to investigate the overall zonal momentum budget, which they found was a balance between topographic form stress and surface wind input in the presence of surface wind stress and buoyancy forcing. Ward and Hogg (2011) further studied the establishment of form stress in a purely wind-driven channel and found that the Coriolis acceleration due to the readjustment of the stratification played an important role in the momentum balance during spinup.

This paper seeks to contrast the mechanisms by which buoyancy and wind forcing influence the input of zonal momentum to a zonally reentrant channel. Given the inevitable balance of momentum at equilibrium, we follow Ward and Hogg (2011) in considering the transient evolution of the system from an initial state with no momentum and look to characterize sources and sinks of momentum. A diapycnal mass flux at the northern and southern boundaries is used to represent the balance between surface buoyancy forcing and diapycnal mixing (hereafter referred to as a buoyancy-forced simulation). This diapycnal flux is combined with a prescribed surface stress to investigate the methods by which buoyancy and wind forcing interact. The different effects of the two forcing regimes is examined by considering the wind- and buoyancy-forced cases both separately and together and by varying their relative and absolute intensities. This work also compares the different force balances that arise from different combinations of buoyancy fluxes and surface wind stress. Particular focus is given to the role of topographic form stress in the zonal momentum balance.

2. Methods

a. Idealized model

We use the isopycnal model of Hallberg and Gnanadesikan (2006), now known as the Generalised Ocean Layer Dynamics (GOLD) model, which solves the primitive equations of motion in isopycnal coordinates using the split time-stepping scheme described in Hallberg (1997). The model is set up in a zonally reentrant channel with three flat, stably stratified layers (of thickness 500, 1500, and 2000 m), with density jumps across the two internal interfaces of 5.0 and 2.5 $\mathrm{kg\,m^{-3}}$. The imposed stratification gives a Rossby radius of deformation of the order of 55 km in the center of the channel; the Rossby radius is thus considerably larger than in the Southern Ocean and thus the magnitude of zonal transport and equilibration times may differ from reality. The horizontal grid cells are square, with 4-km grid spacing in the zonal and meridional directions. The channel is 3200 km long, 1600 km wide, 4 km deep, and contains a Gaussian ridge with a maximum height of 1 km, as shown in Fig. 1b. The variation of the Coriolis parameter with latitude is approximated by a β plane, $f \approx f_0 + \beta y$, with $f_0 = -10^{-4}\,\mathrm{s^{-1}}$ and $\beta = 1.5 \times 10^{-11}\,\mathrm{m^{-1}\,s^{-1}}$,

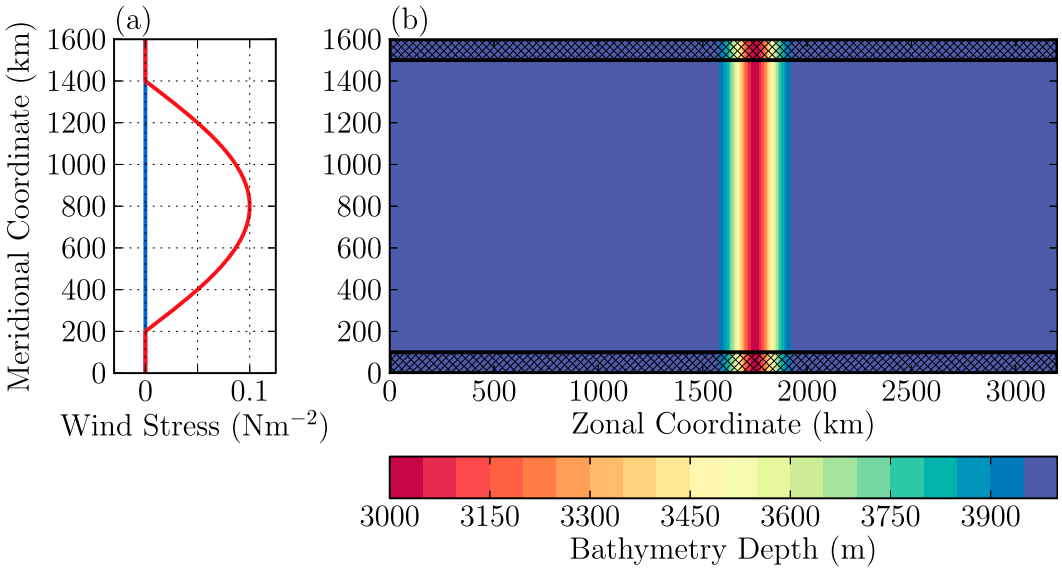

FIG. 1. (a) The meridional wind stress profile (N m^{-2}) and (b) the physical domain. Colors indicate domain depth (m). Shading shows the location of the sponge regions in the buoyancy-forced simulations.

ensuring that the Coriolis acceleration in the channel is comparable to that in the Southern Ocean. We use a frictional bottom drag, with free-slip sidewalls.

Zonal flow in this model is forced in two ways. First, wind forcing is applied via a constant eastward wind stress that contributes to the momentum budget of the upper layer. The distribution of the wind stress does not vary zonally and is greatest at the center of the channel, as shown in Fig. 1a. Second, we use buoyancy forcing to drive an overturning circulation (representative of the lower cell of the MOC) by applying diapycnal fluxes between the three isopycnal layers. This flux is generated by restoring the heights of the isopycnal surfaces toward their prescribed values via water mass transformation across the interfaces. This results in the interfaces moving upward in the south and downward in the north. Forcing occurs in sponge regions covering the northern and southern 100 km of the domain (Fig. 1b).

The rate of water mass transformation in the sponge regions is proportional to the difference between the height of the isopycnal interface and a specified reference height. The reference height for the upper interface (called interface 1 + ½) is 1200 m from the surface at the northern boundary and 50 m from the surface at the southern boundary, while interface 2 + ½ is relaxed to heights of 2000 and 1000 m, respectively. These heights and the relaxation time scale have been chosen so that the intrinsic behavior of the system prevents the interfaces from reaching their prescribed positions, ensuring that water mass transformation occurs even at equilibrium. Transformation in the southern sponge region simulates bottom water formation, while fluxes in the northern sponge region simulate the combined influence of surface heating and diapycnal mixing in the global ocean basins north of the Southern Ocean; we stress that this relaxation is a crude representation of water mass transformation processes, designed to test the fundamental momentum balance of the system with minimal complexity.

To contrast the means by which the wind and buoyancy forcing mechanisms facilitate an input of zonal momentum to the Southern Ocean, we consider three primary simulations: a wind-forced case, a buoyancy-forced case, and a combined forcing case in which both forcings are applied. We conduct two additional wind-forced experiments and two additional buoyancy-forced experiments in which the magnitude of the forcing is doubled and halved while other properties of the simulations are held constant.

b. Momentum balance

To understand the mechanisms governing the response to changes in forcing in these simulations, it is important to quantify the sources and sinks of momentum to the circulation. Following the isopycnal coordinate transformation of Killworth and Nanneh (1994), we derive the momentum budget in this model [consistent with the derivation of Ward and Hogg (2011), but with the addition of diapycnal terms] in the appendix. From this derivation, we obtain the thickness tendency equation Eq. (A13):

$$h_{kt} + (u_k h_k)_x + (v_k h_k)_y + [E]_{k+1/2}^{k-1/2} = 0, \qquad (1)$$

where h_k is the thickness of layer k, $\mathbf{u}_k = [u_k, v_k]$ is the along-isopycnal velocity in that layer, and $[E]_{k+1/2}^{k-1/2}$

denotes the entrainment flux into layer k due to diapycnal processes (see the appendix for details). Partial derivatives with respect to the coordinate axes x, y, or t are represented by subscripts. When integrated zonally, x derivatives cancel, leaving the zonally integrated thickness budget to be

$$\langle h_t \rangle + \langle (vh)_y \rangle + \langle [E]_{k+1/2}^{k-1/2} \rangle = 0, \tag{2}$$

where $\langle \cdot \rangle$ represents the zonal integral. This equation simply notes that the thickness tendency depends upon the combination of diapycnal fluxes and meridional mass transport.

Similarly, the layerwise zonal momentum budget for the kth isopycnal layer is given by Eq. (A15):

$$\begin{aligned}(u_k h_k)_t = &-(u_k^2 h_k)_x - (u_k v_k h_k)_y + f v_k h_k \\ &- M_{kx} h_k + \tau_k^u h_k - [uE]_{k+1/2}^{k-1/2},\end{aligned} \tag{3}$$

where τ^u represents frictional forcing in the zonal direction including viscosity, wind stress, and bottom friction; $M = (p + \rho g z)/\rho_0$ is the Montgomery potential; p is the pressure with respect to the surface; ρ represents density; ρ_0 is a reference density; g is the acceleration due to gravity; and z is the distance to the ocean surface. Following Ward and Hogg (2011), we zonally integrate and convert the Montgomery potential back into pressure (details are provided in the appendix) to give

$$\begin{aligned}\langle (u_k h_k)_t \rangle = &-\langle (u_k v_k h_k)_y \rangle + \langle f v_k h_k \rangle + \langle [p \eta_x]_{k+1/2}^{k-1/2} \rangle \\ &+ \langle \tau_k^u h_k \rangle - \langle [uE]_{k+1/2}^{k-1/2} \rangle,\end{aligned} \tag{4}$$

where $p_{k+1/2}$ and $\eta_{k+1/2}$ are the pressure and height of interface $k + 1/2$. This equation describes fluid acceleration as a balance between the divergence of meridional Reynolds stress, Coriolis acceleration, form stress, friction, and diapycnal fluxes.

Integrating Eq. (4) meridionally yields the balance of sources and sinks of zonal momentum in each layer. The meridional velocity v is zero on the northern and southern boundaries, and so, since the Reynolds stress divergence is an exact derivative, its domainwise integral is zero. Hence, the layerwise-integrated zonal momentum equation is

$$\begin{aligned}\langle\langle (u_k h_k)_t \rangle\rangle = &\langle\langle f v_k h_k \rangle\rangle + \langle\langle [p \eta_x]_{k+1/2}^{k-1/2} \rangle\rangle \\ &+ \langle\langle \tau_k^u h_k \rangle\rangle - \langle\langle [uE]_{k+1/2}^{k-1/2} \rangle\rangle,\end{aligned} \tag{5}$$

where $\langle\langle \cdot \rangle\rangle$ represents the area integral.

The thickness-weighted Coriolis acceleration in each layer is proportional to the northward mass flux in the layer, weighted by the Coriolis parameter. Thus, the integral over all three layers of the Coriolis acceleration is proportional to the total northward mass flux, which must be zero in an equilibrium state so that mass is conserved. Summing Eq. (5) over all three layers is equivalent to integrating zonal momentum over the entire domain. The interfacial form stress and diapycnal fluxes at any interior interface appears with opposing signs in the layer budgets above and below an interface and so contributes nothing to the full-depth integral. Hence, the domain-integrated momentum equation is

$$\begin{aligned}\left\langle\left\langle \left(\sum_{1,2,3} u_k h_k \right)_t \right\rangle\right\rangle = &\left\langle\left\langle \frac{1}{\rho_1} p_{3+1/2} (\eta_{3+1/2})_x \right\rangle\right\rangle \\ &+ \langle\langle \tau^u_{\text{wind}} \rangle\rangle - \langle\langle \tau^u_{\text{bottom}} h_3 \rangle\rangle.\end{aligned} \tag{6}$$

Equation (6) shows that the only sources and sinks of momentum to the system are topographic form stress, surface wind stress, and frictional bottom drag. The Coriolis acceleration, Reynolds stress, and diapycnal terms do not contribute to the domain-integrated momentum balance.

3. Equilibrium state

The evolution of domain-mean eddy kinetic energy (EKE), domain-mean mechanical energy (the sum of available potential and kinetic energy), and zonal volume transport over the spinup period are shown in Figs. 2a–c. These metrics indicate differences between the wind- and buoyancy-forced cases. We find that the buoyancy-forced simulation has lower values of both EKE and mechanical energy and higher zonal volume transport compared with the wind-forced case. The time variation of both energy measures is reduced in the buoyancy-forced case.

A comparison of the combined forcing case with the singly forced cases (Fig. 2) demonstrates which aspects of the circulation depend more heavily on each forcing mechanism. The combined forcing eddy kinetic energy is close to that of the wind-forced simulation, though slightly higher, and has similar variability. The mechanical energy is higher than both the wind- and buoyancy-forced cases, but its variability is comparable to that of the wind-forced simulation. Total zonal transport in the combined forcing case is close to the buoyancy-forced simulation.

The EKE, mechanical energy, and transport in the six singly forced cases and the combined forcing cases are also shown in Figs. 2d–f, scaled relative to the wind-forced simulation where the maximum wind stress is $0.1\,\mathrm{N\,m^{-2}}$

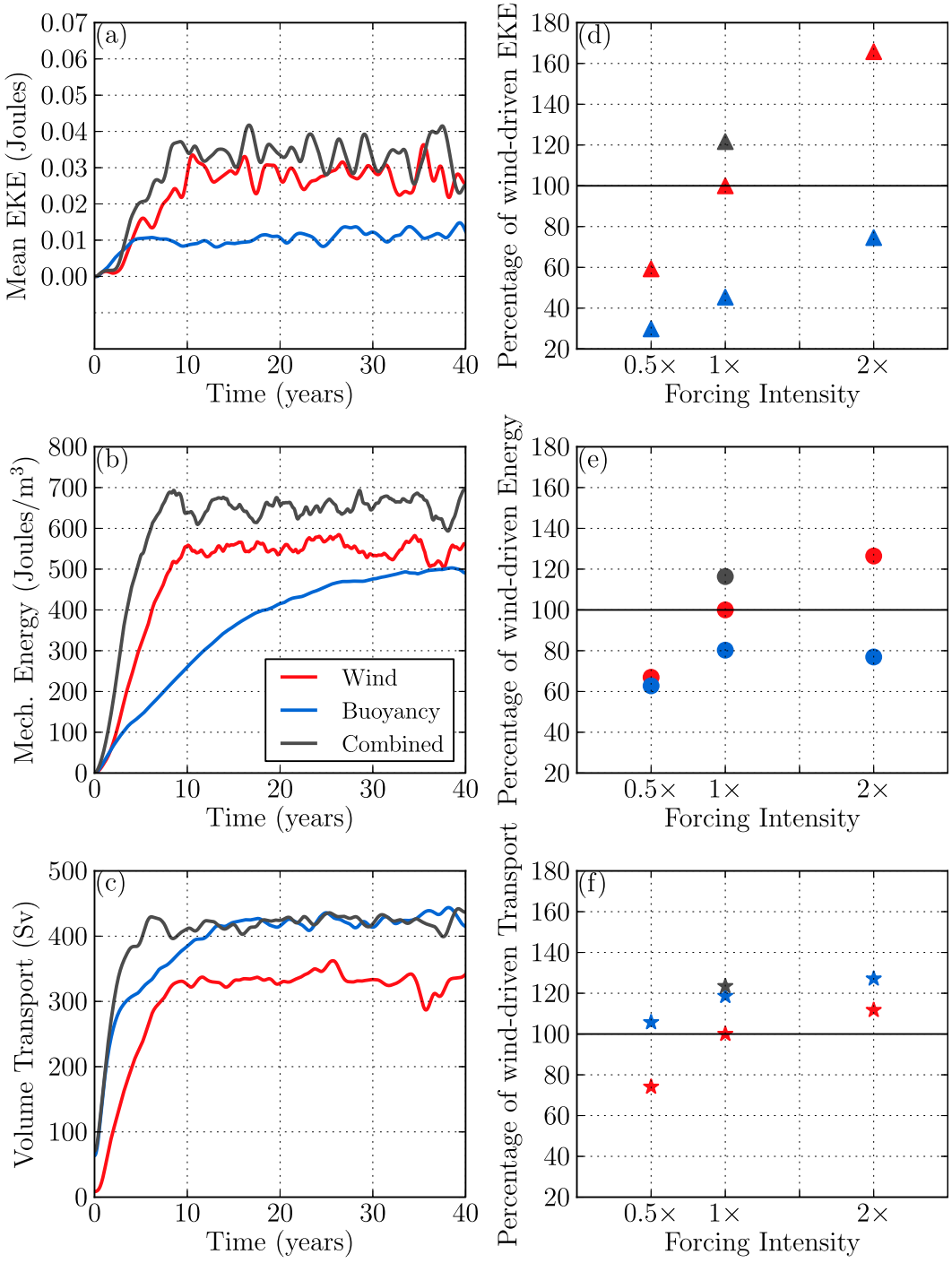

FIG. 2. Time series of (a) domain-mean eddy kinetic energy, (b) domain-mean mechanical energy, and (c) total volume transport in each simulation, filtered by a convolution with a scaled 1-yr Hanning window. The relative values of (d) eddy kinetic energy, (e) domain-mean mechanical energy, and (f) transport in steady state when the forcing intensities are doubled, halved, and combined.

(representative of Southern Ocean values). The extra four singly forced cases show the effect of doubling and halving the forcing intensity (which, in the buoyancy-forced case, equates to halving and doubling the relaxation time scale). It is found that increasing the forcing intensity causes an increase in EKE and transport. The dependence of transport on forcing decreases at higher forcing intensity, consistent with the notion of eddy saturation under both

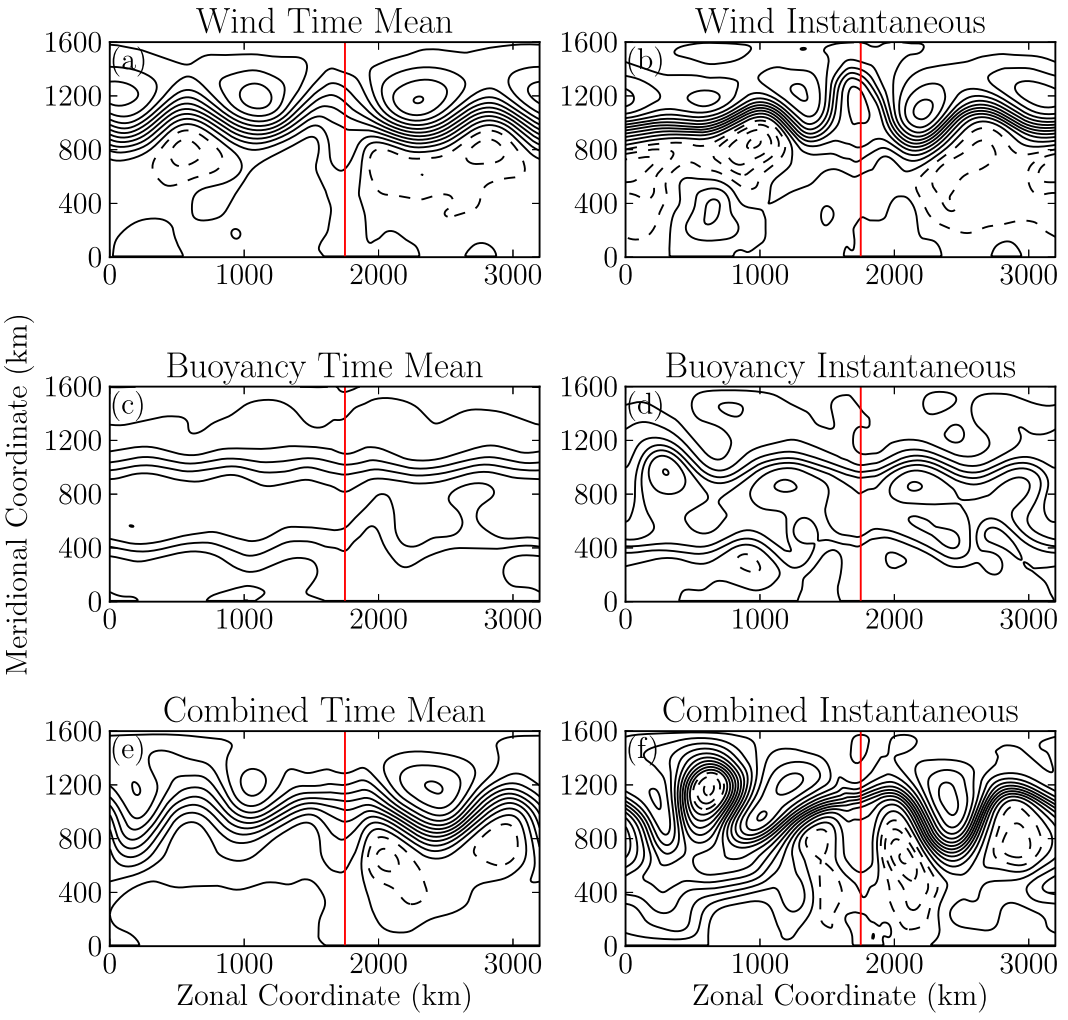

FIG. 3. Barotropic streamfunctions of all three simulations. (left) Time-mean taken over 10 yr in steady state; (right) instantaneous snapshot taken 5 yr after the equilibrated steady state has been reached. (a),(b) Wind-forced simulation, (c),(d) buoyancy-forced simulation, and (e),(f) combined forcing simulation. The red line indicates the location of the maximum height of the ridge in the bottom topography. Contour interval is 20 Sv.

forcing mechanisms. The eddy kinetic energy does not follow this pattern and appears to increase linearly with the forcing strength. The EKE is more sensitive to the wind forcing, while the zonal transport is larger in the buoyancy forcing case.

The time-mean and instantaneous barotropic streamfunctions of each simulation during steady state (Fig. 3) indicate that the turbulent eddy field in the wind-forced and combined forcing cases is visibly more energetic than in the buoyancy-forced case, consistent with Fig. 2a. The velocity structure of the flow also varies significantly over the three simulations. The two simulations with wind forcing exhibit one primary jet that meanders considerably, particularly when passing over topography. However, the buoyancy-forced simulation exhibits two smaller jets with less meandering; the topography appears to have a smaller impact on the barotropic flow.

The steady-state zonal and temporal mean of the overturning circulation and interface positions over each simulation can be seen in Fig. 4. The residual overturning circulation (Fig. 4a) can be inferred from the horizontal arrows, while the vertical arrows indicate the magnitude of the diapycnal flux in the sponge regions. It is evident that an overturning circulation is set up when buoyancy forcing is applied, in contrast to the wind-driven simulation; this result is necessitated by the conservation of mass as illustrated by the consideration of the layer thickness budget [Eq. (2)]. At equilibrium, $\langle h_t \rangle = 0$, the wind-forced case has no entrainment and so meridional transport $\langle (vh)_y \rangle$ is zero. Conversely, the buoyancy-forced and combined cases have a balance

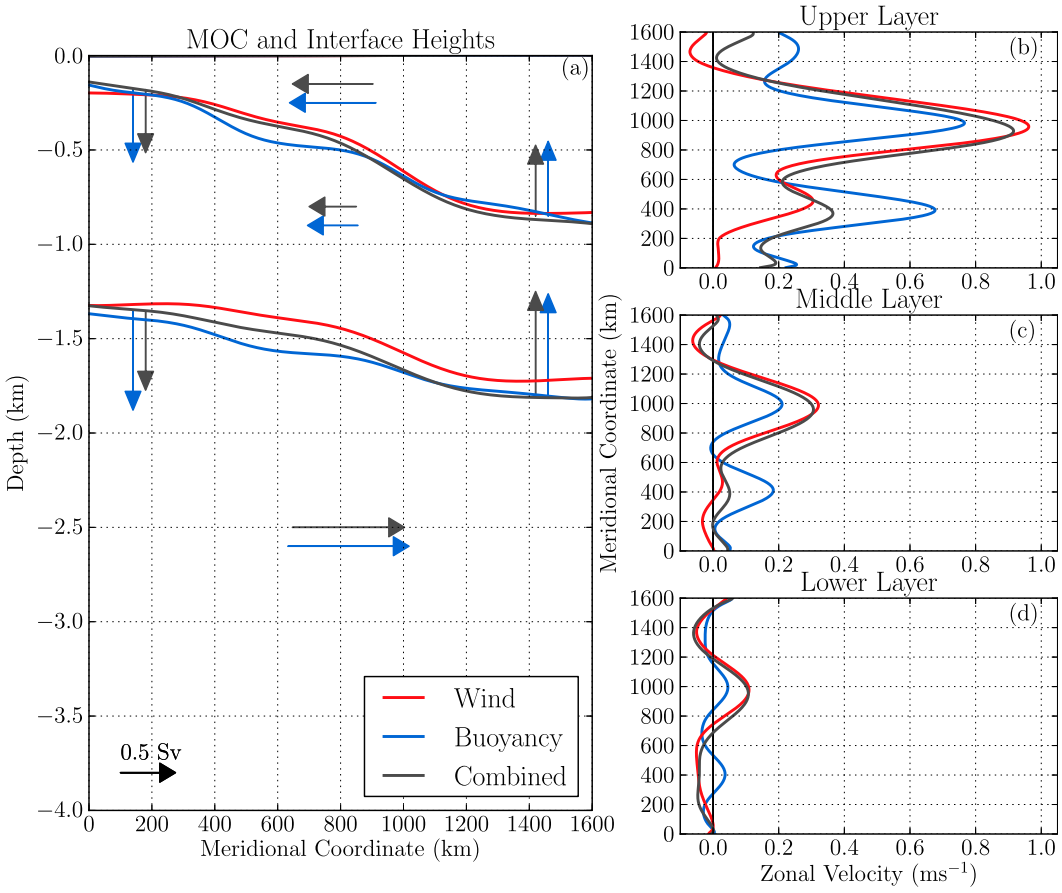

FIG. 4. Mean state of the wind-driven simulations taken as a 10-yr average during steady state. (a) Zonal average of interface heights. The arrows show the overturning circulation; horizontal arrows are scaled to show the domain-mean value of vh outside of the sponge regions and the vertical arrows show the mean entrainment E through each sponge region. No overturning is present in the wind-only-driven simulations. (b) Zonally averaged zonal velocity in the upper layer ($\langle u_1 \rangle$), (c) zonally averaged zonal velocity in the midlayer ($\langle u_2 \rangle$), and (d) zonally averaged zonal velocity in the bottom layer ($\langle u_3 \rangle$).

between the entrainment and meridional transport at equilibrium. The jet structure of the flow (Fig. 4, right-hand panels) features two jets that are strongest at the surface in each simulation. The northern jet dominates when wind forcing is present, while in the buoyancy-forced case the maximum velocity in each jet is roughly equal. When only wind forcing is present, the southern jet is barely visible (consistent with Fig. 3).

4. The momentum budget

a. *Layerwise momentum budgets*

The sources and sinks of momentum in each simulation are investigated using time series of the dominant terms in the layerwise-integrated zonal momentum budget [Eq. (5)]. The acceleration term $(u_k h_k)_t$ as well as the cross-isopycnal momentum flux $[uE]_{k+1/2}^{k-1/2}$ and viscous contributions to the frictional terms were found to be orders of magnitude smaller than the form stress, external stress, and Coriolis terms and so are neglected from the layerwise-averaged momentum balance plots.

1) WIND-FORCED CASE

The evolution of the dominant terms in the domain-averaged zonal momentum equation in each layer is shown in Figs. 5a–c for the spinup of the wind-forced simulation. The Coriolis term (Fig. 5a) is large initially but reduces to oscillate with lower amplitudes about a mean of zero at equilibrium. The Coriolis term is given by fvh and so is proportional to the southward transport. Hence, the initial Coriolis acceleration is associated with the rearrangement of the mass in each layer as the interfaces tilt; associated with the deepening of the upper layer in the north and the shoaling of the upper layer in the south is a northward movement of fluid in the upper

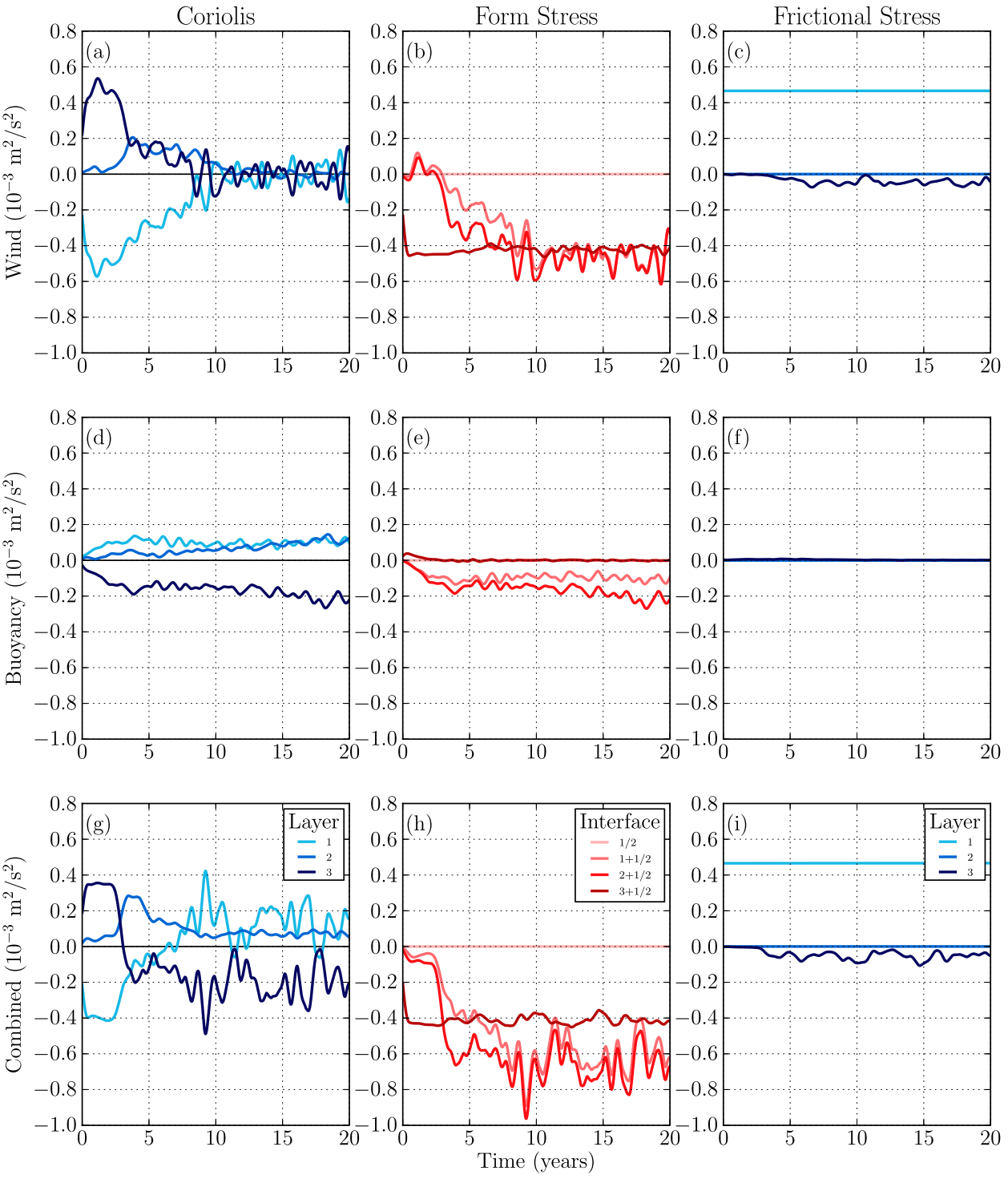

FIG. 5. Time series of the dominant terms in the layerwise zonal momentum balance [Eq. (5)] in (top) the wind-driven simulation, (middle) buoyancy-forced simulation, and (bottom) combined forcing simulation. The time series have been filtered by a convolution with a scaled 1-yr Hanning window. (a),(d),(g) Coriolis acceleration fvh; (b),(e),(h) interfacial and topographic form stress $-p\eta_x$; and (c),(f),(i) wind stress and bottom drag $\tau_{\text{wind}} + \tau_{\text{bottom}}$.

layer and a southward movement of fluid in the lower two layers. In steady state, the Coriolis acceleration consists of small oscillations that cancel in the sum over all the layers.

The topographic form stress $[-p_{3+1/2}(\eta_{3+1/2})_x$; dark red line in Fig. 5b] is always negative, indicating that it is a sink of eastward momentum. The topographic form stress term becomes significant almost instantly after the forcing is applied, implying that forcing projects immediately onto the barotropic mode leading to finite bottom flow and resultant topographic form stress, rather than relying on interfacial form stress to be passed down from the surface through each layer. The magnitude of interfacial form stresses at interfaces 1 + ½ and 2 + ½ (orange/light red lines in Fig. 5b) is initially small, but grows over the spinup period, stabilizing when the Coriolis term becomes negligible. This spinup takes approximately 10 yr, consistent with the spinup of an energetic eddy field (Fig. 2a) that is a prerequisite for significant interfacial form stress. In steady state, fluctuations in the interfacial form stress balance those in the Coriolis term within each layer.

Initially, topographic form stress appears to balance the Coriolis acceleration in layer three caused by the rearrangement of the height of the interface 2 + ½. As the Coriolis term decreases, the topographic form stress remains constant, balancing the difference between the interfacial form stress at the interface above and the oscillations in the Coriolis acceleration. The stress on the upper layer is provided by the wind and is constant in time (Fig. 5c). There is an additional frictional stress in the bottom layer, provided by bottom drag, which initiates when the flow in the bottom layer is sufficiently large.

In steady state, the dominant balance in the upper layer is between the applied wind stress and the interfacial form stress. In the midlayer, the balance is between form stress at the top and bottom interfaces, while in the lowest layer the dominant balance is between interfacial form stress from interface 2 + ½ and topographic form stress. Variations in the Coriolis term balance variations in the interfacial form stress within each layer. Hence, at equilibrium, the zonal momentum from the wind forcing of the upper layer is transferred through to the bottom layer via interfacial form stress where it is dissipated through topographic form stress. These results are consistent with the equilibrium results of Munk and Palmén (1951) and Stevens and Ivchenko (1997), as well as the transient adjustment reported by Ward and Hogg (2011).

2) BUOYANCY-FORCED CASE

With only the overturning circulation present (Figs. 5d–f), the Coriolis term increases in magnitude over the first 15 yr to a steady negative value of about $2 \times 10^{-3}\,\mathrm{m^2\,s^{-2}}$ in the lower layer and smaller positive values in the upper- and midlayers; the sum of this term across all three layers is zero. Multiplying by the length of the domain, this result suggests the establishment of an overturning circulation with total transport of 0.64 Sv. This overturning is equivalent to ~5 Sv for a Southern Ocean length channel, which is smaller but a similar order of magnitude to observational estimates (e.g., ~20 Sv; Lumpkin and Speer 2007).

The Coriolis acceleration in the buoyancy-forced simulation is very different from that in the wind-driven simulation shown in Fig. 5a. With buoyancy forcing, meridional transport in each layer results from the entrainment term in the thickness budget [Eq. (2)]; it is initially small, as the entrainment is balanced by changes in thickness, but is finite at equilibrium. This meridional transport leads to Coriolis acceleration in the opposite direction of that in the initial stages of the spinup in the wind-forced case in the top and bottom layers (but the same direction in the midlayer). Thus, the buoyancy forcing generates overturning of the opposite sense to the wind forcing, despite both cases accumulating eastward momentum at equilibrium (Fig. 4). Within each layer, the Coriolis term (Fig. 5d) is balanced by the interfacial form stress (Fig. 5e) and these terms sum to zero in the depth-integrated momentum budget.

The consequence of these Coriolis terms is that flow is initially accelerated toward the east in the surface layer and toward the west in the two lowest layers. As such, the buoyancy forcing acts to create a baroclinic shear in the flow. The westward lower-layer flow is slowed by processes that act to damp flow (such as topographic form stress and bottom drag) allowing these processes to contribute net eastward momentum. This sink of westward momentum acts as a source of eastward momentum for the system as a whole. Accordingly, the topographic form stress is initially positive, also contributing eastward momentum that balances the immediate Coriolis acceleration, but decays to zero after several years. During the time period when the topographic form stress is nonzero, there is a small, positive imbalance of these terms, allowing the eastward momentum of the system to increase. However, the topographic form stress is only significant for the first 2 yr (Fig. 5e), whereas the transport increases over the first 20 yr of the simulation (Fig. 2c). Bottom drag (Fig. 5f) is the only other term present that contributes to the domain-integrated momentum budget. While the contribution of bottom drag to the momentum budget appears negligible in Fig. 5f, it is generally positive (i.e., it acts as a source of eastward momentum by acting to damp the lower-layer flow), and we make the case below that it is a significant cumulative

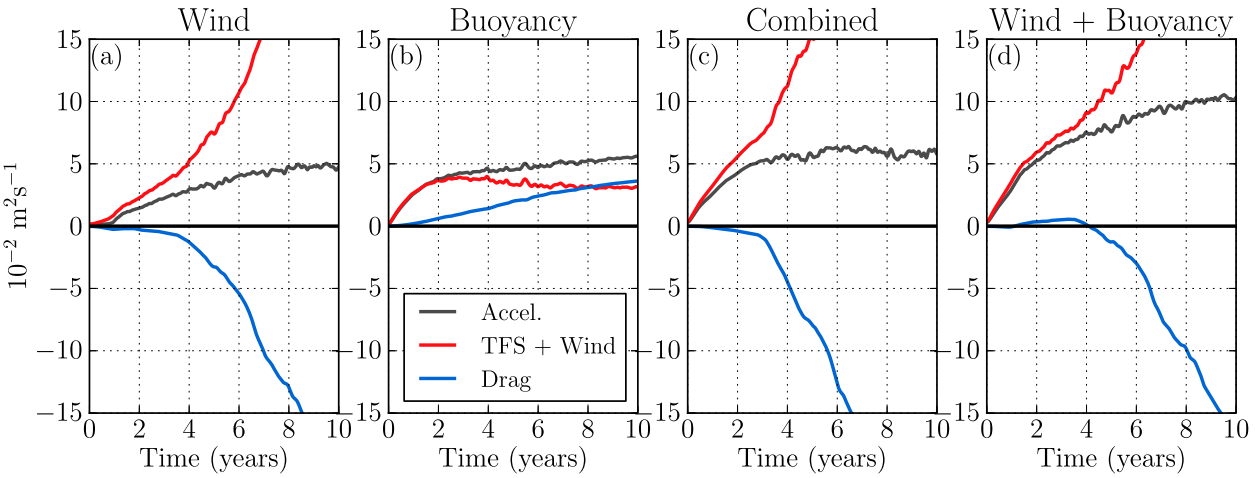

FIG. 6. Cumulative time integrals of the terms in the domain-integrated zonal momentum balance in (a) the wind-driven simulation, (b) buoyancy-forced simulation, (c) combined forcing simulation, and (d) linear sum of the buoyancy-forced and wind-driven simulations. The gray line shows thickness-weighted acceleration $\sum_{k=1}^{3}(u_k h_k)_t$, the red line show topographic form stress $p\eta_x + \tau_{\text{wind}}$, and the blue line shows bottom drag τ_{bottom}.

contribution to eastward momentum over the course of the simulation.

3) COMBINED FORCING CASE

When both wind and buoyancy forcing are applied, the dominant terms in the momentum balance (Figs. 5g–i) of each of the simulations with one forcing mechanism can be superimposed (Figs. 5a–f). The Coriolis term (Fig. 5g) is initially positive in the lowest two layers and negative in the upper layer, suggesting that the fluid quickly responds to wind forcing to readjust so that the interfaces tilt as shown in Fig. 4a. After 5 yr, the signs of the Coriolis acceleration in the uppermost and lowest layers switch, so that the net meridional motion of the fluid is the overturning circulation induced by the buoyancy forcing.

The interfacial form stresses at interfaces 1 + ½ and 2 + ½ (Fig. 5h) increase over the first 5 yr in a manner similar to both of the singly forced cases. After this time, the mean value of interfacial form stress at each interface is roughly equal to the sum of the wind- and buoyancy-forced cases. Thus, interfacial form stress appears to depend linearly upon both forcing mechanisms. The behavior of topographic form stress, surface wind stress, and bottom drag all appear to mimic the wind-forced case, implying that the domain-integrated budget is dominated by direct momentum input from the wind in the combined forcing case.

b. Domain-integrated momentum budget

Figure 6 shows the accumulated contribution of the sources and sinks of momentum to the entire system and the resulting acceleration of the zonal flow over the first decade of each simulation. As topographic form stress and wind stress are large and opposing when wind forcing is applied, we elect to show only the residual of these terms. When only wind forcing is applied (Fig. 6a), topographic form stress is insufficient to balance the wind stress and so the residual is positive. This residual generates the net eastward acceleration during spinup but is balanced by bottom drag once the system equilibrates. Equilibration takes ~10 yr in this case; it is notable that while the primary balance is between wind stress and topographic form stress, the biggest difference between the equilibrating and equilibrated states is the increase in bottom friction in the latter.

When only buoyancy forcing is applied (Fig. 6b), the initial acceleration is more rapid than in the wind-driven case, and >80% of the acceleration occurs within 2 yr. The mechanism of acceleration is due to topographic form stress damping the westward bottom flow set up by the baroclinic shear response. The drag on the bottom westward flow acts as a positive input of eastward momentum to the system as a whole. However, as the interfaces adjust to the forcing, topographic form stress diminishes, and after 8 yr frictional bottom drag overtakes topographic form stress as the primary cumulative source of eastward momentum. From this point onward, equilibration is more gradual and is not complete after 20 yr (Fig. 5e).

The combined forcing case (Fig. 6c) follows the form of the wind-forced simulation, but the rate of acceleration owing to the residual of the form stress and the wind is greater in the initial phases; spinup time is of the order of 5 yr, which is faster than either of the singly forced cases. As the momentum injected by the wind forcing is fixed, this result implies that the topographic form stress

is influenced by the presence of buoyancy forcing in the first few years. Furthermore, a linear summation of the momentum forcing in the wind- and buoyancy-forced cases (Fig. 6d) predicts the topographic form stress of the combined forcing case in the first 3 yr, but gives the incorrect sign of the bottom drag for this period. We conjecture that the rapid spinup results from the greater energy input to the system owing to the combination of forcing mechanisms, which drives the eddy field and resultant interfacial form stress to reach equilibrium faster.

5. Discussion and conclusions

Buoyancy forcing, representing the combined effects of surface fluxes and interior mixing, can drive a quasi-steady zonal circulation in a zonally reentrant channel reminiscent of the Antarctic Circumpolar Current. The zonal transport can be predicted from thermal wind balance alone, but such a balance does not reveal the source of momentum or the mode of transient adjustment. Here, we have demonstrated that during the spinup of a system forced by buoyancy forcing, buoyancy fluxes are balanced by a residual overturning that advects fluid northward in the bottom layer and southward in the upper layers, implying a Coriolis acceleration that is eastward in the surface layers and westward in lower layers. Flow in the deep ocean is preferentially damped by a combination of topographic form stress and bottom drag, leaving a net eastward flow. Thus, while buoyancy forcing does not directly inject momentum into the flow, it induces a meridional circulation that acts as a sink of westward momentum from the flow (which contributes depth-integrated eastward momentum to the flow) through the solid lower boundary. The buoyancy-induced meridional circulation also redistributes momentum vertically, delivering eastward momentum to the surface via Coriolis acceleration.

The momentum budget in the buoyancy-forced case has been contrasted with that of the wind-forced case. During spinup, wind forcing generates tilting density interfaces that induce a meridional flux in the opposite direction of the buoyancy-forced case and so a Coriolis acceleration is present in the zonal momentum balance. The topographic form stress is established almost instantaneously by projection of the forcing onto the barotropic mode and is then constant over the duration of the spinup process.

Acknowledgments. EH gratefully acknowledges the support of an A. L. Hales Scholarship provided by RSES. AMH was supported by an Australian Research Council Future Fellowship FT120100842. This research was undertaken on the NCI National Facility in Canberra, Australia, which is supported by the Australian Commonwealth Government. Our thanks to Ryan Abernathey, Andy Thompson, and two anonymous reviewers for constructive comments on the first draft of this paper.

APPENDIX

Derivation of Isopycnal Coordinate Momentum Equations

The momentum and continuity equations are written in thickness-weighted isopycnal coordinates, following the derivations of Killworth and Nanneh (1994) and Ward and Hogg (2011). Consider the incompressible hydrostatic equations of motion in z coordinates:

$$\mathbf{u}_t + \mathbf{u}\cdot\nabla\mathbf{u} + f\hat{k}\times\mathbf{u} = -\frac{\nabla p}{\rho_0} + \tau, \tag{A1}$$

$$p = g\int_z^0 \rho\, dz, \tag{A2}$$

$$\nabla\cdot u = 0, \tag{A3}$$

$$\rho_t + \mathbf{u}\cdot\nabla\rho = Q, \tag{A4}$$

where all quantities are as defined in section 2b.

The coordinate transformation to density is performed by transforming from the basis (x, y, z, t) to (x', y', ρ, t'), where $x' = x$, $y' = y$, and $t' = t$. To simplify the hydrostatic equation, pressure is replaced by the Montgomery potential $M = (p + \rho g z)/\rho_1$, where the reference density ρ_1 is the surface density. By definition, $p_x = M_{x'}\rho_1$ (noting that the derivatives are evaluated along z and ρ surfaces) and likewise $p_y = M_{y'}\rho_1$. The hydrostatic equation [Eq. (A2)] becomes

$$M_\rho = \frac{gz}{\rho_1}. \tag{A5}$$

The cross-isopycnal velocity w can be written (dropping primes hereafter) as

$$w = Qz_\rho + uz_x + vz_y + z_t. \tag{A6}$$

The continuity equation [Eq. (A3)] yields

$$(uz_\rho)_x + (vz_\rho)_y + (Qz_\rho + z_t)_\rho = 0. \tag{A7}$$

For any scalar quantity a,

$$\frac{Da}{Dt} = u_t + ua_x + va_y + Qa_\rho. \tag{A8}$$

Therefore, the horizontal momentum equations [Eq. (A1)] in isopycnal coordinates become

$$u_t = -uu_x - vu_y + fv - M_x + \tau^u - Qu_\rho, \quad \text{(A9)}$$

$$v_t = -uv_x - vv_y - fu - M_y + \tau^v - Qv_\rho, \quad \text{(A10)}$$

which are the tendency equations for u and v. The zonal momentum budget is connected to its thickness-weighted form by multiplying the continuity equation [Eq. (A7)] by u and adding the thickness-weighted zonal momentum equation [Eq. (A9)]. The result is

$$(uz_\rho)_t = -(u^2 z_\rho)_x - (uvz_\rho)_y + z_\rho fv - M_x z_\rho + \tau^u z_\rho - (uQz_\rho)_\rho, \quad \text{(A11)}$$

yielding the thickness-weighted zonal momentum equation in isopycnal coordinates.

Now, consider the stratified reentrant ocean channel described in section 2, recalling that here $u(x, y, \rho)$ and $v(x, y, \rho)$ are constant within an isopycnal layer. By integrating the thickness-weighted continuity equation [Eq. (A7)] across an isopycnal layer, the conservation of thickness equation is obtained:

$$h_t + (uh)_x + (vh)_y + [Qz_\rho]_{k+1/2}^{k-1/2} = 0. \quad \text{(A12)}$$

Set $[E]_{k+1/2}^{k-1/2} = [Qz_\rho]_{k+1/2}^{k-1/2}$ to be the entrainment flux into layer k. The conservation of thickness Eq. (A12) becomes

$$h_t + (uh)_x + (vh)_y + [E]_{k+1/2}^{k-1/2} = 0. \quad \text{(A13)}$$

To analyze the thickness-weighted zonal momentum budget, the zonal momentum equation [Eq. (A11)] is integrated over each isopycnal layer (following Killworth and Nanneh 1994):

$$\int_{k+1/2}^{k-1/2} (uz_\rho)_t \, d\rho = \int_{k+1/2}^{k-1/2} [(u^2 z_\rho)_x - (uvz_\rho)_y + z_\rho fv - M_x z_\rho + \tau^u z_\rho - (uQz_\rho)_\rho] \, d\rho, \quad \text{(A14)}$$

which can be evaluated as

$$(u_k h_k)_t = -(u_k^2 h_k)_x - (u_k v_k h_k)_y + fv_k h_k - M_{kx} h_k + \tau_k^u h_k - [uE]_{k+1/2}^{k-1/2}, \quad \text{(A15)}$$

where uE in a layer represents the diapycnal entrainment across the bounding interfaces $[uQz_\rho]_{k+1/2}^{k-1/2}$. This calculation is not straightforward since Q is defined on interfaces, and u is defined inside layers. The term uE is thus defined so that

$$[uE]_{k+1/2}^{k-1/2} = h_k[u_{k-1}(Q_{k-1/2})^- - u_k(Q_{k-1/2})^+ - u_k(Q_{k+1/2})^- + u_{k+1}(Q_{k+1/2})^+]. \quad \text{(A16)}$$

Integrating Eq. (A15) zonally along the channel, and noting that the zonal gradient of the Reynolds stress term makes no contribution, we obtain

$$0 = \int_0^L (u_k^2 h_k)_x \, dx = [u_k^2 h_k]_0^L = 0, \quad \text{(A17)}$$

where L is the zonal coordinate of the eastern boundary of the domain. Hence, the zonally integrated, zonal thickness-weighted momentum budget for the kth layer becomes

$$\langle (u_k h_k)_t \rangle = -\langle (u_k v_k h_k)_y \rangle + \langle fv_k h_k \rangle - \langle M_{kx} h_k \rangle + \langle \tau_k^u h_k \rangle - \langle [uE]_{k+1/2}^{k-1/2} \rangle. \quad \text{(A18)}$$

The pressure term $\langle M_{kx} h_k \rangle$ is found below to be entirely because of form stress imparted on a layer at its boundaries. Form stress may be explicitly evaluated as follows: The Montgomery potential is replaced by pressure, and since p is only well defined on interfaces, average values are used in the following. From the vertical hydrostatic equation,

$$p_z = -g\rho \Rightarrow p_{k+1/2} = p_{k-1/2} + g\rho_k h_k. \quad \text{(A19)}$$

From the definition of M,

$$M_k = \frac{1}{2\rho_1}(p_{k+1/2} + p_{k-1/2}) + \frac{g\rho_k}{2\rho_1}(\eta_{k+1/2} + \eta_{k-1/2}). \quad \text{(A20)}$$

Therefore, set $P_k = [1/(2\rho_1)](p_{k+1/2} + p_{k-1/2})$. Then, following Ward and Hogg (2011) and using the hydrostatic equation [Eq. (A2)],

$$h_k \nabla M^k = h_k \nabla P + h_k \nabla \frac{g\rho^k}{2\rho_1}(\eta_{k+1/2} + \eta_{k-1/2}), \quad \text{(A21)}$$

$$= \nabla h_k P_k - \frac{1}{\rho_1} p_{k-1/2} \nabla \eta_{k-1/2} + \frac{1}{\rho_1} p_{k+1/2} \nabla \eta_{k+1/2}. \quad \text{(A22)}$$

Since the x derivative term makes no contribution as it is integrated around a closed loop, the zonally integrated, thickness-weighted, zonal momentum equation can be written as

$$\langle (u_k h_k)_t \rangle = -\langle (u_k v_k h_k)_y \rangle + \langle fv_k h_k \rangle + \left\langle \frac{1}{\rho_1} [p\eta_x]_{k+1/2}^{k-1/2} \right\rangle + \langle \tau_k^u h_k \rangle - \langle [uE]_{k+1/2}^{k-1/2} \rangle, \quad \text{(A23)}$$

which is identical to Eq. (4). The terms on the right-hand side represent, respectively, the Reynolds stress divergence, Coriolis acceleration, form stress, frictional terms, and cross-isopycnal momentum flux by entrainment.

REFERENCES

Borowski, D., R. Gerdes, and D. Olbers, 2002: Thermohaline and wind forcing of a circumpolar channel with blocked geostrophic contours. *J. Phys. Oceanogr.,* **32,** 2520–2540, doi:10.1175/1520-0485-32.9.2520.

Gent, P. R., W. G. Large, and F. O. Bryan, 2001: What sets the mean transport through Drake Passage? *J. Geophys. Res.,* **106,** 2693–2712, doi:10.1029/2000JC900036.

Gnanadesikan, A., and R. Hallberg, 2000: On the relationship of the circumpolar current to Southern Hemisphere winds in coarse-resolution ocean models. *J. Phys. Oceanogr.,* **30,** 2013–2034, doi:10.1175/1520-0485(2000)030<2013:OTROTC>2.0.CO;2.

Hallberg, R., 1997: Stable split time stepping schemes for large-scale ocean modelling. *J. Comput. Phys.,* **135,** 54–65, doi:10.1006/jcph.1997.5734.

——, and A. Gnanadesikan, 2006: The role of eddies in determining the structure and response of the wind-driven Southern Hemisphere overturning: Results from the Modelling Eddies in the Southern Ocean (MESO) project. *J. Phys. Oceanogr.,* **36,** 2232–2252, doi:10.1175/JPO2980.1.

Hogg, A. M., 2010: An Antarctic Circumpolar Current driven by surface buoyancy forcing. *Geophys. Res. Lett.,* **37,** L23601, doi:10.1029/2010GL044777.

Killworth, P. D., and M. M. Nanneh, 1994: Isopycnal momentum budget of the Antarctic Circumpolar Current in the Fine Resolution Antarctic Model. *J. Phys. Oceanogr.,* **24,** 1201–1223, doi:10.1175/1520-0485(1994)024<1201:IMBOTA>2.0.CO;2.

Lumpkin, R., and K. Speer, 2007: Global ocean meridional overturning. *J. Phys. Oceanogr.,* **37,** 2550–2562, doi:10.1175/JPO3130.1.

Mazloff, M. R., R. Ferrari, and T. Schneider, 2013: The force balance of the Southern Ocean meridional overturning circulation. *J. Phys. Oceanogr.,* **43,** 1193–1208, doi:10.1175/JPO-D-12-069.1.

Meredith, M. P., and A. M. Hogg, 2006: Circumpolar response of Southern Ocean eddy activity to a change in the southern annular mode. *Geophys. Res. Lett.,* **33,** L16608, doi:10.1029/2006GL026499.

——, and Coauthors, 2011: Sustained monitoring of the Southern Ocean at Drake Passage: Past achievements and future priorities. *Rev. Geophys.,* **49,** RG4005, doi:10.1029/2010RG000348.

Munday, D. R., L. C. Allison, H. L. Johnson, and D. P. Marshall, 2011: Remote forcing of the Antarctic Circumpolar Current by diapycnal mixing. *Geophys. Res. Lett.,* **38,** L08609, doi:10.1029/2011GL046849.

——, H. L. Johnson, and D. P. Marshall, 2013: Eddy saturation of equilibrated circumpolar currents. *J. Phys. Oceanogr.,* **43,** 507–532, doi:10.1175/JPO-D-12-095.1.

Munk, W. H., and E. Palmén, 1951: Note on the dynamics of the Antarctic Circumpolar Current. *Tellus,* **3,** 53–55, doi:10.1111/j.2153-3490.1951.tb00776.x.

Rintoul, S., C. W. Hughes, and D. Olbers, 2001: The Antarctic Circumpolar Current system. *Observing and Modelling the Global Ocean,* G. Siedler, J. Church, and J. Gould, Eds., *Ocean Circulation and Climate,* Vol. 77, Academic Press, 271–302.

Shakespeare, C. J., and A. M. Hogg, 2012: An analytical model of the response of the meridional overturning circulation to changes in wind and buoyancy forcing. *J. Phys. Oceanogr.,* **42,** 1270–1287, doi:10.1175/JPO-D-11-0198.1.

Stevens, D. P., and V. O. Ivchenko, 1997: The zonal momentum balance in an eddy-resolving general circulation model of the Southern Ocean. *Quart. J. Roy. Meteor. Soc.,* **123,** 929–951, doi:10.1002/qj.49712354008.

Straub, D. N., 1993: On the transport and angular momentum balance of channel models of the Antarctic Circumpolar Current. *J. Phys. Oceanogr.,* **23,** 776–782, doi:10.1175/1520-0485(1993)023<0776:OTTAAM>2.0.CO;2.

Ward, M. L., and A. M. Hogg, 2011: Establishment of momentum balance by form stress in a wind-driven channel. *Ocean Modell.,* **40,** 133–146, doi:10.1016/j.ocemod.2011.08.004.